

Gasdynamics in NGC 4736

Qiu-Sheng Gu¹, Xin-Hao Liao¹, Jie-Hao Huang¹, Qin-Yue Qu¹, and Hongjun Su²

¹ Department of Astronomy, Nanjing University, Nanjing 210093, China

² Purple Mountain Observatory, Nanjing 210008, China

Received ; accepted

Abstract. New test-particle simulations have been performed to study the secular evolution of the gaseous distribution in NGC 4736. We find that the distribution of gas clouds can be understood in the frame of perturbation induced by a nuclear oval potential, in addition to a spiral-like potential. Our experiments show that both inner and outer rings are stable structures located at the inner Lindblad resonance (ILR) and the outer Lindblad resonance (OLR), respectively, in agreement with the observations of NGC 4736. One of our simplified simulations indicates that both nuclear starburst and orbital resonance might be needed for keeping the inner ring stable for a long period. We have introduced a symplectic algorithm in the orbit integration. Its stronger stability allows us to adopt a rather large time step to save computational time. Substitution of a viscous force for cloud-cloud interactions proves adequate in the case of NGC 4736.

Key words: galaxies: spiral – galaxies: evolution – galaxies: kinematics and dynamics – galaxies: structure – galaxies: individual(NGC 4736) – methods: numerical

1. Introduction

NGC 4736 (M94) is a bright, nearby Sab galaxy¹, which is notable for a faint outer HI ring of radius 4 arcmin to 6 arcmin, and an inner bright ring of HII region with enhanced gas density at 45 arcsec (Lynds 1974; Beckman et al. 1991). Beckman et al. (1991) found that the bulge position angle ($\sim 20^\circ$) was very different from that of the disc ($\sim 120^\circ$), strong evidence for non-axisymmetry in the bulge of NGC 4736, and suggested that triaxiality of the bulge played an important dynamical role in fuelling star formation.

Send offprint requests to: Q.-S Gu, e-mail:postcstd@nju.edu.cn

¹ The Hubble distance is still uncertain, we adopt 6.3 Mpc in this paper, so that 1 arcmin is equal to 1.8 kpc.

Discussion of the origin of these rings is separated into two groups. On one hand, van der Kruit(1974, 1976) and Sanders & Bania(1976) suggested that the ring-like structures in NGC 4736 are the observational signature of recent nuclear explosive events. On the other hand, Schommer & Sullivan (1976) and Bosma et al. (1977) proposed that the rings result from tight winding of spiral arms and are tracers for the principle orbital resonance regions. Athanassoula et al. (1982) thought that NGC 4736 is in fact the prototype of rings located at Lindblad resonances in an oval potential.

Gerin, Casoli & Combes (1991) have shown that both inner HII and outer HI rings could form in a slight barred potential. The possible existence of such an oval was first discussed by Bosma, van der Hulst & Sullivan (1977) and Kormendy (1979) and more recently by Huang, Gu & Su (1993). As pointed out by the authors themselves, the model of Gerin, Casoli & Combes has two main drawbacks. Their outer ring is too wide (cf. their Fig. 10b), so that it was in fact associated with both corotation at about 4.5 kpc and OLR at about 8.0 kpc. The second drawback is that their inner ring disappears after 3 Gyrs. The aim of this paper will be to produce a model devoid of these drawbacks.

Here, we present our numerical experiments on gas clouds in NGC 4736 based on the test-particle method. We replace the process of cloud-cloud collision with the viscous force widely used in the study of accretion disks and introduce the symplectic algorithm, which has proven of strong stability, in our simulations. Both inner and outer ring structures turned out to be quite stable after 4.0 Gyr, and are associated with the inner Lindblad resonance (ILR) and outer Lindblad resonance(OLR) for a long duration, respectively.

In Sect.2, we describe the construction of the model potential of NGC 4736, and the method of replacing the process of collision between gas clouds. The computational method, namely, the near-symplectic algorithm, is described in Sect.3, and in Sect.4 we present the simulation results of the gasdynamics in NGC 4736. Finally, we give the discussions and conclusions in Sect.5 and 6.

2. The new simulations

We assume in our new simulations that the motions of the gas clouds are mainly dominated by the following two physical processes: the galaxy's gravitational field and the mutual collision between gas clouds. Note that we neglect the self-gravity of the gas cloud, which may have an important effect in some cases.

2.1. The gravitational field

Following the basic approach, the galactic potential consists of two parts, an axisymmetric background and a non-axisymmetric perturbing potential. We assume that the background potential has four components: a spherical bulge, a thick disk, a thin disk, and a spherical halo. Both the density distribution of the bulge and of the halo take the form

$$\rho = \begin{cases} \frac{\rho_0}{2\pi} \left(1 - \frac{r}{r_c}\right), & r \leq r_c, \\ 0, & r > r_c. \end{cases} \quad (1)$$

which implies an underlying bulge gravitational potential of the form

$$U_B = \begin{cases} -2.0G\rho_0r^2\left(\frac{1}{3} - \frac{r}{4r_c}\right), & r \leq r_c, \\ -G\rho_0r_c^3/6r, & r > r_c. \end{cases} \quad (2)$$

The halo potential U_H has the same form as U_B . The thick and thin disks are assumed to be Toomre disks (Toomre, 1963), and have the form

$$U_D(r) = -\frac{GM_D}{(r_c^2 + r^2)^{1/2}}, \quad (3)$$

We take the perturbing potential as the same as that used in Roberts & Hausman's simulations(1984).

$$U_1(r, \theta, t) = U_D(r) \frac{A}{5} \frac{r_c^2 r^2}{(r_c^2 + r^2)^2} \cos[2\theta - 2\Omega_p t + \Phi(r)]. \quad (4)$$

where $\Phi(r)$, the phase of the maximum perturbation, is determined by

$$\Phi(r) = 2 \log(1 + (r/r_0)^j) / (j \tan i_0), \quad (5)$$

In the above equations, r_c is a constant canonical radius, Ω_p is pattern speed, M_D the total mass of the Toomre disk, r_0 a characteristic radius where the perturbing potential changes from barlike to spiral-like. The power j determines how sharply the shift from barlike to spiral perturbation occurs with increasing r , and i_0 is the pitch angle of the spiral. In our model, r_0 , j , and i_0 are set to be 1.0kpc, 5, and 10° , respectively.

Now we can construct a mass model of NGC 4736 by fitting the observed rotation curve with the model potentials mentioned above. The rotation curve of NGC 4736 has the following characteristics: a steep rise from the nucleus to 0.25 arcmin, a turn-over region from 0.25 to 0.5

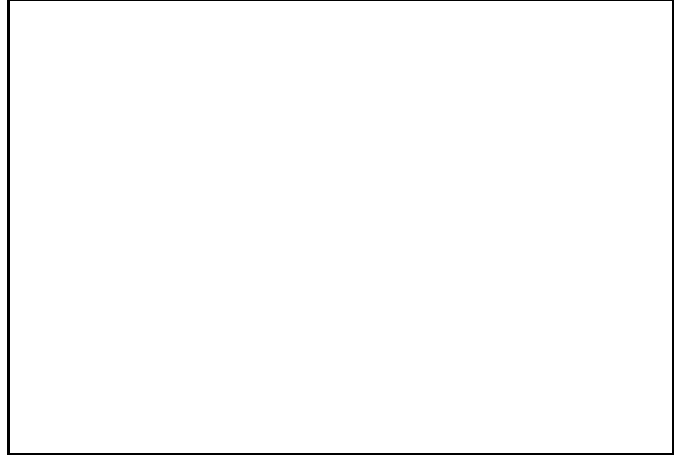


Fig. 1. Rotation curve model of NGC 4736

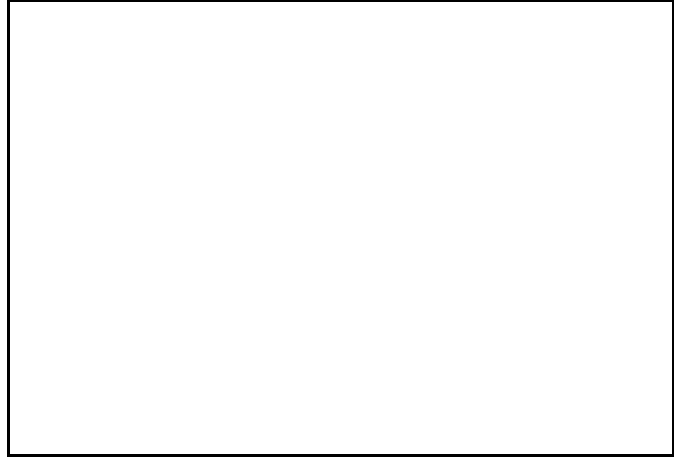


Fig. 2. Circular angular velocity (Ω) and Lindblad precession frequencies ($\Omega \pm \kappa/2$) vs. radius for the rotation curve model of NGC 4736

arcmin, a constant-velocity region from 0.5 to 4.0 arcmin and a decreasing-velocity region from 4.0 to 6.0 arcmin (Schommer & Sullivan 1976 ; Bosma et al. 1977). The mass parameters, determined this way, of the bulge, thick disk, thin disk and halo are 0.005, 0.032, 0.11, and 0.11 kpc^3/Myr^2 , respectively, and the constant canonical radii for these four components are 0.30, 0.45, 2.50, and 8.20 kpc, respectively. Fig.1 gives the rotation curve model corresponding to the unperturbed gravitational field defined by the above parameter values, which is almost in keeping with that derived from optical and radio observations. The standard Lindblad precession frequencies for this rotation curve are shown in Fig. 2.

The equation of motion of gas clouds in the potential $U(x, y, t)$ can be written as

$$\begin{cases} \frac{dx}{dt} = \frac{\partial H}{\partial \dot{x}}, & \frac{d\dot{x}}{dt} = -\frac{\partial H}{\partial x}, \\ \frac{dy}{dt} = \frac{\partial H}{\partial \dot{y}}, & \frac{d\dot{y}}{dt} = -\frac{\partial H}{\partial y}, \end{cases} \quad (6)$$

where, H , the Hamiltonian of the gas cloud, is represented by

$$H = H(x, y, \dot{x}, \dot{y}, t) = \frac{1}{2}(\dot{x}^2 + \dot{y}^2) + U(x, y, t), \quad (7)$$

\dot{x} and \dot{y} are the canonical conjugate variables of x and y , respectively.

2.2. The mutual collisions between gas clouds

The cloud-cloud collision is obviously related to the following parameters: the gas density, the velocity dispersion, the collision cross-section, the constitution of matter, the differential rotation, the included collision angle, etc. Therefore, it is difficult to formulate the collision processes exactly in numerical simulations. The effect of the mutual collision between gas clouds was treated as a simple fractional reduction of the relative velocities first by Schwarz (1981, 1984). In our present numerical experiments, we introduce a dissipative viscous force to simulate the effect of collision, expressed by the following formula in the well-known α -disk (Shakura and Sunyaev 1973; Pringle 1981),

$$F = \alpha C_s \Sigma h r \frac{d\Omega}{dr}, \quad (8)$$

where, α is a constant and $0 < \alpha < 1$; C_s the local sound velocity; Σ the cloud surface density; Ω the local angular velocity; and h the spiral thickness. For the gas clouds in a galaxy, C_s is just the local velocity dispersion. As a first-order approximation, we take $\mathbf{v} - \mathbf{v}_0$ as C_s , where \mathbf{v} and \mathbf{v}_0 is the local velocity and the local unperturbed circular rotation speed, the initial number density of gas clouds Σ_0 as Σ , and the local unperturbed circular rotation Ω_0 as Ω . So, we have

$$\mathbf{F} = \alpha(\mathbf{v} - \mathbf{v}_0)\Sigma_0 h r \frac{d\Omega_0}{dr} \quad (9)$$

to replace the effect of collision between gas clouds. Obviously, \mathbf{F} is a small quantity of first-order magnitude as compared with the unperturbed gravitational force. With the addition of \mathbf{F} , the motion equation of a single gas cloud on the circle of radius r becomes

$$\begin{cases} \frac{dx}{dt} = \frac{\partial H}{\partial \dot{x}}, & \frac{d\dot{x}}{dt} = -\frac{\partial H}{\partial x} + 2\pi r F_x, \\ \frac{dy}{dt} = \frac{\partial H}{\partial \dot{y}}, & \frac{d\dot{y}}{dt} = -\frac{\partial H}{\partial y} + 2\pi r F_y, \end{cases} \quad (10)$$

where F_x and F_y are the components of \mathbf{F} in the directions of x and y , respectively.

3. The computational method

For the numerical computation of the Hamiltonian system, we could adopt traditional methods such as Runge-Kutta. But most of the traditional numerical methods will cause a linear variation of the system energy with time, contrary to the theoretical results for Hamiltonian systems.

It is known that the Hamiltonian flow preserves its symplectic structure (Arnold, 1978). Based on this property, a symplectic algorithm for Hamiltonian systems has been developed (Ruth 1983; Feng 1984). Its obvious advantage over the traditional methods is in the aspect of the long-term dynamical evolution of Hamiltonian system, i.e. no secular change in the system energy.

For the Hamiltonian system

$$\begin{cases} \dot{q} = \frac{\partial H}{\partial p}, \\ \dot{p} = -\frac{\partial H}{\partial q}, \end{cases} \quad (11)$$

with Hamiltonian function

$$H = H(p, q) = T(p) + V(q), \quad (12)$$

where $p, q \in R^n$ are a set of canonical conjugate variables, its phase flow is represented by

$$\begin{pmatrix} p(t) \\ q(t) \end{pmatrix} = \exp[(t - t_0)D_H] \begin{pmatrix} p(t_0) \\ q(t_0) \end{pmatrix}, \quad (13)$$

where the differential operator D_H is defined by the Poisson bracket $\{\cdot, \cdot\}$ as follows

$$D_H = \{\cdot, H\} \quad (14)$$

and $\exp[(t - t_0)D_H]$ is the exponential transformation of D_H . Let the integration time-step be τ , both of the following step-transition operators

$$g_1^\tau = \exp(\tau D_T) \exp(\tau D_V) \quad (15)$$

$$\check{g}_1^\tau = \exp(\tau D_V) \exp(\tau D_T) \quad (16)$$

are first-order symplectic integrators. It is easy to prove that both

$$g_2^\tau = g_1^\tau \circ \check{g}_1^\tau \quad (17)$$

and

$$\check{g}_2^\tau = \check{g}_1^\tau \circ g_1^\tau \quad (18)$$

are second-order symplectic algorithms. Higher-order symplectic algorithms can be constructed from a certain number of second-order symplectic algorithms (Yoshida, 1990).

The difference scheme corresponding to g_2^τ is

$$\begin{cases} q_{k+\frac{1}{2}} = q_k + \frac{\tau}{2} \frac{\partial T(p)}{\partial p} \Big|_{p=p_k}, \\ p_{k+1} = p_k - \tau \frac{\partial V(q)}{\partial q} \Big|_{q=q_{k+\frac{1}{2}}}, \\ q_{k+1} = q_{k+\frac{1}{2}} + \frac{\tau}{2} \frac{\partial T(p)}{\partial p} \Big|_{p=p_{k+1}}, \end{cases} \quad (19)$$

where (p_{k+1}, q_{k+1}) and (p_k, q_k) are the numerical solutions of the Hamiltonian flow (13) at time $t = (k+1)\tau$ and $t = k\tau$, respectively, and $p_0 = p(t_0)$, $q_0 = q(t_0)$.

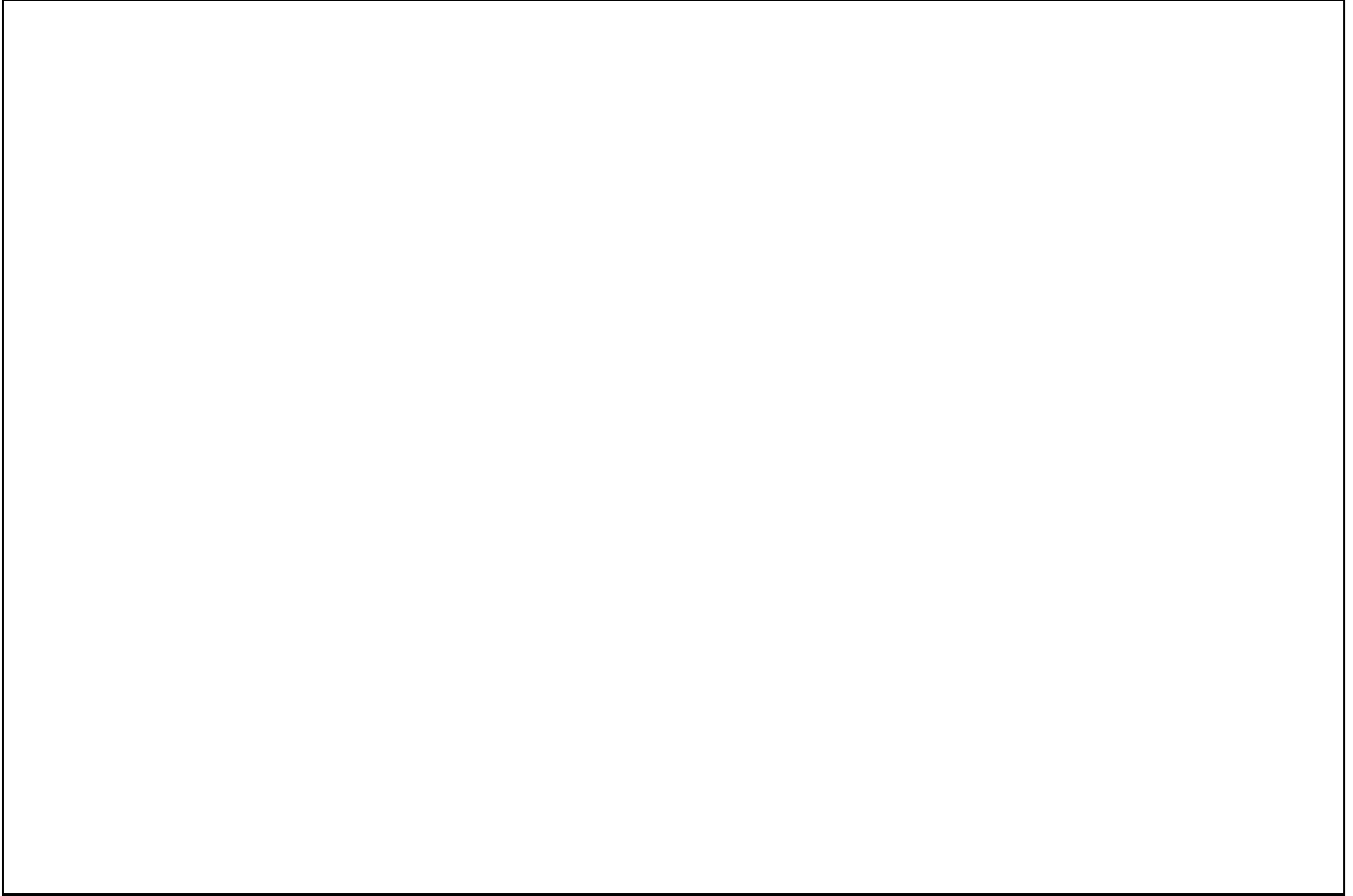


Fig. 3. Time evolution of the gas clouds in our model. The time epochs for a, b, c, d, e, and f are 50 Myr, 200 Myr, 400 Myr, 1.0 Gyr, 2.0 Gyr and 4.0 Gyr, respectively.

If we consider the small dissipative effect, then equation (11) becomes

$$\begin{cases} \dot{q} = \frac{\partial H}{\partial p}, \\ \dot{p} = -\frac{\partial H}{\partial q} + \varepsilon F(p, q), \end{cases} \quad (20)$$

Since ε is a small quantity, we could replace the solution of the second equation (20) by an Euler flow. Hence the difference scheme (19) changes to

$$\begin{cases} q_{k+\frac{1}{2}} = q_k + \frac{\tau}{2} \frac{\partial T(p)}{\partial p} \Big|_{p=p_k}, \\ p_{k+1} = p_k - \tau \left[-\frac{\partial V(q)}{\partial q} + \varepsilon F(p, q) \right] \Big|_{p=p_k, q=q_{k+\frac{1}{2}}}, \\ q_{k+1} = q_{k+\frac{1}{2}} + \frac{\tau}{2} \frac{\partial T(p)}{\partial p} \Big|_{p=p_{k+1}}, \end{cases} \quad (21)$$

This kind of treatment causes the truncation error of (21) to be of order $\max[O(\tau^3), O(\tau^2\varepsilon)]$. Obviously, we can ensure that the scheme (21) is second-order if $\varepsilon < \tau$, and we will use this scheme in our simulation.

It should be noticed that the “leap-frog” difference scheme used in the N -body simulation is also symplectic and second-order. But its stable interval is very small in comparison with scheme (21).

4. Results

At the beginning of each simulation, 10000 gas clouds are uniformly distributed in the disk with 10 kpc radius. Each cloud is given with a local circular rotation velocity, along with a peculiar velocity selected from a two-dimensional Gaussian distribution whose one-dimensional dispersion is 5 km s^{-1} .

With the amplitude of the spiral perturbation $A = 0.4$, the pattern speed $\Omega_p = 0.03$, and the viscous coefficient $\alpha = 0.001$, the dynamical evolution of gas clouds with time is given in Fig.3. It is clearly shown that when time $t = 50 \text{ Myr}$, Fig. 3a, a faint ring-like structure of radius 1.1kpc emerges in the central region; with increasing time, more and more gas particles move inward and accumulate at the ring region. At $t = 400 \text{ Myr}$, the inner stable ring becomes prominent, roughly located at the ILR with a radius of 1.1 kpc, see Fig. 3c. At the same time, in the outer part of the disk, an outer ring is formed as the result of tight winding of spiral arms. It is stable and of low-density with radius 7.5 kpc to 10.0 kpc, a location near the OLR and beyond. It is interesting to notice that both inner and outer ring structures are stable for durations

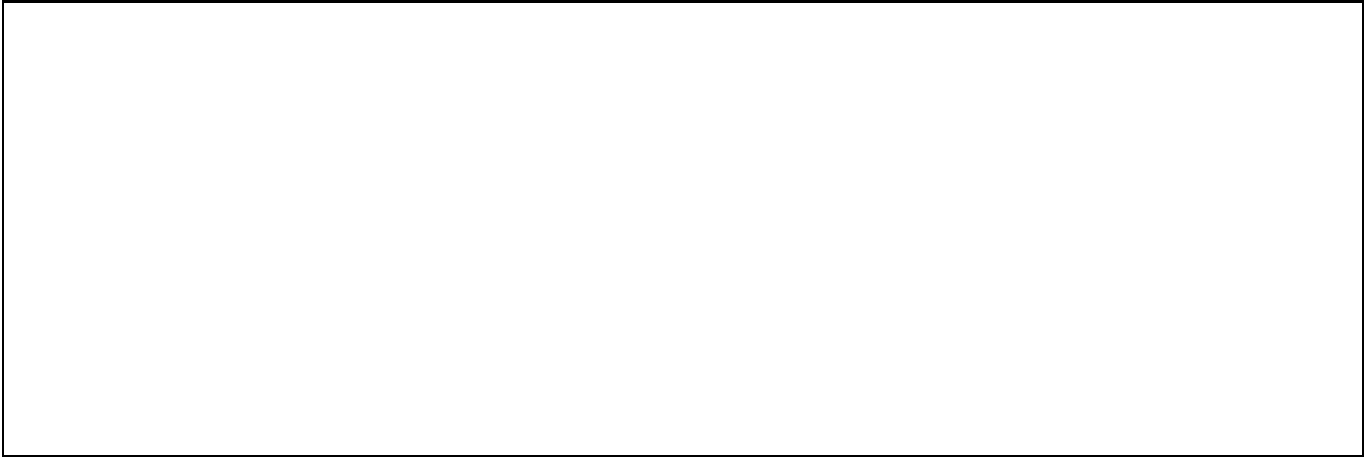


Fig. 4. Time evolution of the gas clouds, to which within the ILR region some radial motions are added when $\Sigma > \Sigma_c$. The time epochs for a, b and c are 500 Myr, 1.0 Gyr, and 3.6 Gyr, respectively.

of 100 Myr to 800 Myr, fixed onto the ILR and OLR, respectively, in agreement with the observations of NGC 4736.

After 1.0 Gyr, the inner ring moves inward further, to a radius of about 0.7kpc, see Fig. 3d, and stays there till 4.0 Gyr, see Fig. 3f. Meanwhile, the outer ring appears narrower, but remains in the OLR region.

5. Discussion

5.1. Validity

The results obtained in Fig 3. are conditional on the absence of other complicated processes during the cloud-cloud collision, e.g., the formation of giant molecular clouds and subsequent instabilities, star formation or massive star bursts, and such follow-up processes as heating by stars, stellar wind, protostellar jets and poststellar explosions. Indeed, such processes could be triggered when the surface density of gas clouds becomes high enough (Elmegreen 1994), and the motions and thermodynamic state of the gas clouds could be affected (Krugel & Tutukov 1993). Obviously, our present simulation code will not be valid in such case.

We give a very simplified example. Beckman et al (1991) suggest that starburst activities around the nucleus of NGC 4736 can produce an outflow motion of $\sim 30\text{km s}^{-1}$, as observed by van der Kruit (1976), Thus we add radial motions ($\sim 30\text{km s}^{-1}$) to some of the gas clouds inside the ILR when the surface density Σ is higher than a critical value $\Sigma_c = \alpha \frac{\kappa c}{3.36G}$ (Toomre 1964, Cowie 1981, Kennicutt 1989). This might be a way to understand the possible influence of star formation on the distribution of gas clouds in the ILR region. The simulation obtained in this case is shown in Fig 4. It is interesting to find that the inner ring remains stable at the ILR location of about 1.1 – 1.2 kpc even after 3.6 Gyr. Although this approach

to simulating the effect of star formation is very crude, it does give a clue that the debate on the origin of the ring structures in NGC 4736 mentioned in Sect. 1 could be reconciled in that both nuclear explosion, an event probably similar to massive starburst, and orbital resonance are needed for keeping the inner ring stable for a long period of time. More work on this matter is under consideration.

5.2. Modelling of the cloud-cloud interactions

In comparison with others, and beyond the potential adopted for NGC 4736, we have modified both the orbit integrator and the modelling of the cloud-cloud interactions. To see whether the latter is the basic factor improving our results, as suggested by Lia Athanassoula (1995, private communication), we have repeated one of Schwarz's simulations (1984), using exactly the same potential as he, but our model for cloud-cloud interactions. The results are shown in Fig 5 with the viscous coefficient $\alpha = 0.0001$. It is interesting to note that the depopulation of the L_4, L_5 Lagrangian points is much more rapid than Schwarz's results, shown in his Fig 6 (1984). The outer ring forms after four bar rotations, and becomes almost circular and stable after six bar rotations. The same structures formed in Schwarz's simulation after twenty bar rotations. It appears that the basic difference between Schwarz's simulation and ours is the time evolution and the time scale for stabilization. Thus, we believe that the different modelling of the cloud-cloud interactions might be the dominant factor responsible for the improvement in our results.

5.3. The approximation

An important approximation in our numerical experiments was to keep the surface density, Σ , in eqn.(8) constant during the time evolution of gas clouds. Apparently, it is far from being the case, as the simulation indicated.



Fig. 5. Time evolution of the gas clouds, using Schwarz's potential but our model for cloud-cloud interactions. The time epochs in bar rotations are 2, 4, 6, 8, 10, and 20 for frames a, b, c, d, e, and f, respectively.

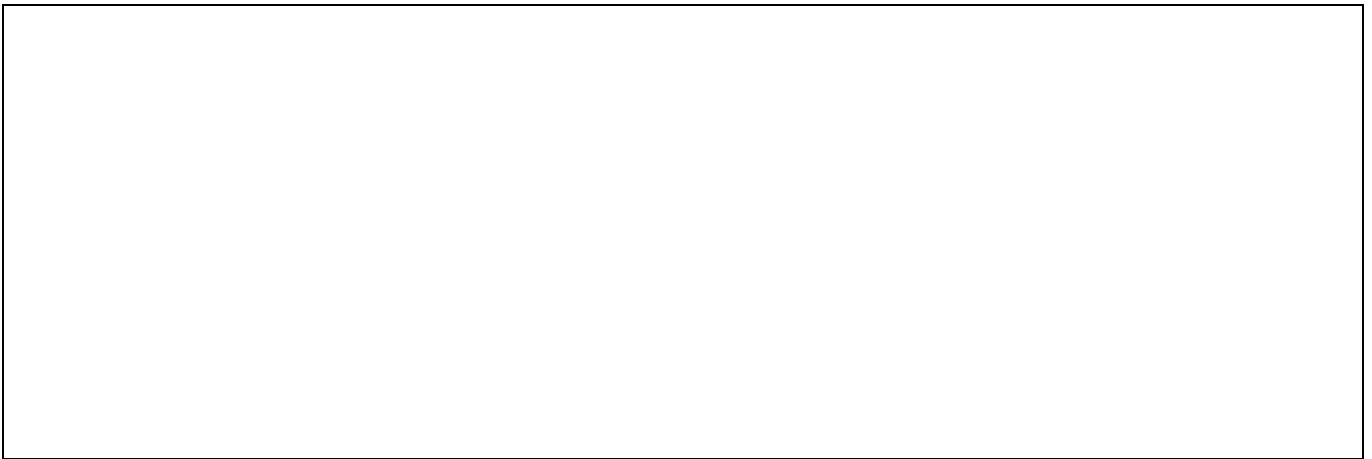


Fig. 6. Time evolution of the gas clouds, same parameters as those in Fig. 3 were used except that the variation of Σ was tracked at each time step. The time epochs for a, b and c are 50 Myr, 400 Myr and 1.0 Gyr, respectively.

We have examined the effect of this approximation. Instead of keeping constant surface density, Σ_0 , a more time-consuming simulation has been performed, in which the variation of surface density was tracked for each step. One such simulation is shown in Fig 6. As compared with those in Fig. 3, one can find major differences in the inner ring, which moves closer to the nucleus and gathers many more gas clouds. On the other hand, the approximation has little effect on the outer ring structure.

Though tracking the variation of Σ is more realistic, that more gas clouds assemble near the galactic nucleus may not be true. As pointed out in Sect.5.1, when the gas density exceeds the critical value Σ_c , the process of star formation or even starburst must be considered instead. The resulting superwind might prohibit the gas clouds from moving inward, as our simple simulation in Fig 4 indicated. So, it might not be reasonable to track the variation of Σ without considering the processes of intense star formation and the subsequent superwind. In other words, the approximation made in the present simulation might not be too bad.

6. Conclusions

In this paper, we present a new "sticky particle" model of NGC 4736, which has three improvements over previous models for this galaxy: (1) The orbit integrator; (2) the potential adopted for the galaxy; and (3) the different modelling of cloud-cloud interactions. The main advantages are as follows: (1) The numerical experiments show that both inner and outer rings in NGC 4736 are stable structures located at the ILR and OLR, respectively, more in agreement with the observations. The simulations overcome the drawbacks described in Sect. 1; (2) The symplectic algorithm has an advantage over the usual leapfrog method in the time step taken, which could save a lot of computational time during the simulations; (3) The major improvement is due to the different modelling of the cloud-cloud interactions with the viscous force as suggested in Sect. 5.2.

Our very simplified simulation gives us a clue that both nuclear explosions caused by starburst activities and orbit resonance might be needed to keep the inner ring stable. A more realistic way to introduce the process of star formation as well as the cloud-cloud collision into our simulation is under consideration.

Acknowledgements. We would like to thank the referee, Dr. E. Athanassoula, for her careful reading our manuscript and her instructive suggestions, that significantly improve our analyses in this paper. We would also like to thank the anonymous language corrector for improving and correcting our English presentation. This research was supported by grants from National Science and Technology Commission and National Natural Science Foundation of China.

References

- Arnold V.I., 1978, *Mathematical Method of Classical Mechanics*, Springer, New-York.
- Athanassoula, E., Bosma, A., Cr ez e, M., & Schwarz, M.P., 1982, *A&A*, 107, 101
- Beckman J. E., Varela A. M., Munoz-Tunon C., Vilchez J. M., Cepa J., 1991 *A&A*, 245, 436
- Bosma A., van der Hulst J. M., Sullivan III W. T., 1977, *A&A*, 57, 373
- Cowie L. L., 1981, *ApJ*, 245, 66
- Elmegreen B. G., 1994, *ApJ* 425, L73
- Feng K. 1985 in *Proc. 1984 Beijing Symp. Diff. Geom. and Diff. Eq.* Ed. K. Feng, Science Press, Beijing, 42
- Gerin M., Casoli F., Combes F., 1991, *A&A*, 251, 32
- Lynds B. T., 1974, *ApJSS*, 28, 267
- Huang J. H., Gu Q. S., Su H. J., 1993, in *Mass-induced Activities in Galaxies*, ed I. Shlosman, Cambridge University Press, P.119
- Kennicutt R. C., 1989, *ApJ*, 344, 685
- Kormendy J., 1979, *ApJ*, 227, 714
- Krugel E., Tutukov A. V., 1993, *A&A*, 275, 416
- Pringle J. E., 1981, *ARA&A*, 19,137
- Roberts W. W., Huntley J. M., van Albada G.D., 1979, *ApJ*, 233, 67
- Roberts W. W., Hausman M. A., 1984, *ApJ*, 277, 744
- Ruth R. D., 1983, *IEEE, Trans. on Nuc. Sci.*, NS-30, 2669
- Sanders R. H., Bania T. M., 1976, *ApJ*, 204, 341
- Schommer R. A., Sullivan III W. T., 1976, *Astrophys. Lett.*, 17, 191
- Schwarz M. P., 1981, *ApJ*, 247, 77
- Schwarz M. P., 1984, *MNRAS*, 209, 93
- Shakura N. I., Sunyaev R. A., 1973, *A&A*, 24, 337
- Toomre A., 1963, *ApJ*, 138, 385
- Toomre A., 1964, *ApJ*, 139, 1217
- van der Kruit P. C., 1974, *ApJ*, 188, 3
- van der Kruit P. C., 1976, *A&A*, 52, 85
- Yoshida H., 1990, *Phys. Letters A*, 150, 262